On multi-spectral quantitative photoacoustic tomography in diffusive regime



2012 Inverse Problems 28 025010

(http://iopscience.iop.org/0266-5611/28/2/025010)

Inverse Problems **28** (2012) 025010 (13pp) doi:10.1088/0266-5611/28/2/025010

# On multi-spectral quantitative photoacoustic tomography in diffusive regime

**Guillaume Bal**[1] **and Kui Ren**[2]

[1] Department of Applied Physics and Applied Mathematics, Columbia University, New York, NY 10027, USA
[2] Department of Mathematics, University of Texas at Austin, Austin, TX 78712, USA

E-mail: gb2030@columbia.edu and ren@math.utexas.edu

Received 12 September 2011, in final form 6 December 2011
Published 20 January 2012
Online at stacks.iop.org/IP/28/025010

**Abstract**
The objective of quantitative photoacoustic tomography (qPAT) is to reconstruct the diffusion, absorption and Grüneisen thermodynamic coefficients of heterogeneous media from knowledge of the interior absorbed radiation. It has been shown in Bal and Ren (2011 *Inverse Problems* **27** 075003), based on diffusion theory, that with data acquired at one given wavelength, all three coefficients cannot be reconstructed uniquely. In this work, we study the multi-spectral qPAT problem and show that when multiple wavelength data are available, all coefficients can be reconstructed simultaneously under minor prior assumptions. Moreover, the reconstructions are shown to be very stable. We present some numerical simulations that support the theoretical results.

(Some figures may appear in colour only in the online journal)

## 1. Introduction

In photoacoustic tomography (PAT), near infrared (NIR) light propagates into a medium of interest. As a fraction of the incoming light energy is absorbed, the medium heats up. This results in mechanical expansion and the generation of compressive (acoustic) waves. The acoustic waves propagate to the boundary of the medium where they are measured. From knowledge of these (time-dependent) acoustic measurements, one attempts to reconstruct the diffusion, absorption and Grüneisen thermodynamic properties of the medium of interest [2, 7, 19, 31, 33, 36, 39, 47, 55–57].

The reconstruction problem in PAT is a two-step process. In the first step, one reconstructs the absorbed energy map (multiplied by a coefficient), $H$ defined in (2) below, from the measured acoustic signals on the surface of the medium. This is a relatively well-known inverse source problem for the wave equation that has been extensively studied in the past [1, 16, 21, 22, 25–28, 32, 34, 37, 39, 40, 50–53]. In the second step, often called quantitative PAT (qPAT), the objective is to reconstruct the diffusion coefficient $D$ in (1), the absorption

  

coefficient $\sigma$ in (1) and the Grüneisen coefficient $\Gamma$ in (2), from the reconstructed energy data $H$. This step has recently attracted significant attention from both mathematical [3, 4, 8–10] and computational [11, 17, 18, 20, 24, 23, 35, 45, 46, 59, 61] perspectives. Mathematically, the reconstruction problem in this step is very similar to the diffuse optical tomography (DOT) problem except that in DOT we have boundary current data, while here in qPAT we have interior absorbed energy data. The use of interior data improves the stability, and thus the resolution, of the reconstruction significantly. This is the main advantage of PAT over DOT.

Most of the studies in the past have assumed that the Grüneisen coefficient is a constant and is *known* so that only the absorption and diffusion coefficients are to be reconstructed. As recently pointed out in [17, 19, 48], it is more realistic to consider $\Gamma$ as a function of space. In this work, we treat $\Gamma$ also as an unknown. We thus aim at both $\Gamma$ and the optical coefficients. Note that unlike the reconstruction of the absorption coefficient $\sigma$ and the diffusion coefficient $D$, the reconstruction of $\Gamma$ is a linear inverse problem since the data $H$ we have are linearly proportional to $\Gamma$. This means that if both $\sigma$ and $D$ are known, then we can simply solve the diffusion equation (1) and compute the energy $E = \sigma u$. Then $\Gamma$ is reconstructed as $\Gamma = H/E$.

The work in [9] has shown that with data at only one wavelength, the reconstruction of the three coefficients simultaneously is not unique. In fact, only two of the three coefficients can be reconstructed without other *a priori* information. The objective of this work is exactly to reconstruct all three coefficients by using measured data of different wavelengths and *a priori* information on the form of the coefficients. We show that the reconstruction can be done when the coefficients take specific forms. One specific case of practical importance is that if the dependence of the coefficient on the spatial variable and on the wavelength variable can be separated, then they can be reconstructed with spectral data stably.

The paper is structured as follows. In section 2, we reformulate the inverse problem of quantitative PAT in the setting of multiple wavelength illuminations and present uniqueness and stability theory regarding the inverse problem in simplified settings. We then present in section 3 numerical procedures to reconstruct the unknown coefficients. We present some numerical simulation results with synthetic data in section 4. Conclusions and further remarks are offered in section 5.

## 2. Uniqueness and stability results

Let us denote by $X$ a bounded domain in $\mathbb{R}^d$ ($d = 2, 3$) with the smooth boundary $\partial X$, and $\Lambda \subset \mathbb{R}_+$ the set of wavelengths at which the interior data are constructed. In the diffusive regime, the density of photons at the wavelength $\lambda$, $u(\mathbf{x}, \lambda)$ solves the following diffusion equation:

$$\begin{aligned} &-\nabla \cdot D(\mathbf{x}, \lambda)\nabla u(\mathbf{x}, \lambda) + \sigma(\mathbf{x}, \lambda)u = 0, \quad X \times \Lambda \\ &u(\mathbf{x}, \lambda) = g(\mathbf{x}, \lambda), \quad \partial X \times \Lambda, \end{aligned} \tag{1}$$

where $D(\mathbf{x}, \lambda) > 0$ and $\sigma(\mathbf{x}, \lambda) > 0$ are the wavelength-dependent diffusion and absorption coefficients, respectively, and $g(\mathbf{x}, \lambda)$ is the illumination pattern in photoacoustic experiments. The wavelength-dependent interior data constructed from the inversion of the acoustic problem are given by

$$H(\mathbf{x}, \lambda) = \Gamma(\mathbf{x}, \lambda)\sigma(\mathbf{x}, \lambda)u(\mathbf{x}, \lambda), \quad (\mathbf{x}, \lambda) \in X \times \Lambda, \tag{2}$$

where $\Gamma(\mathbf{x}, \lambda) > 0$ is the non-dimensional Grüneisen coefficient that relates the absorbed optical energy $\sigma u$ to the increase in pressure $H$. The thermodynamic coefficient $\Gamma$ measures the photoacoustic efficiency of the medium.

The problem of multi-spectral qPAT is to reconstruct the coefficients $D(\mathbf{x}, \lambda)$, $\sigma(\mathbf{x}, \lambda)$ and $\Gamma(\mathbf{x}, \lambda)$ from interior data of the form (2). The results in [9] state that without further

*a priori* information, we cannot uniquely reconstruct all three coefficients. In fact, only two quantities related to the three coefficients, i.e. the functionals $\chi(\mathbf{x},\lambda)$ and $q(\mathbf{x},\lambda)$, defined in (5) below can be reconstructed. The objective of this work is to show that when data of multiple wavelengths are available, we can recover the uniqueness in the reconstructions with relatively little additional *a priori* information. To obtain results that are as general as possible, we allow the diffusion and absorption coefficients to be arbitrary functions of the wavelength and assume that the Grüneisen coefficient can be written as the product of a function of space and a function of wavelength. More precisely, the coefficients take the following form:

$$D = D(\mathbf{x},\lambda), \quad \sigma = \sigma(\mathbf{x},\lambda), \quad \Gamma(\mathbf{x},\lambda) = \gamma(\lambda)\Gamma(\mathbf{x}), \tag{3}$$

where $\gamma(\lambda)$ is a function assumed to be *known*. This assumption is not sufficient to guarantee unique reconstructions. We need to assume a little more on the coefficients. Our main assumption is as follows.

(A1) There exist two *known* wavelengths $\lambda_1, \lambda_2 \in \Lambda$ so that $D(\mathbf{x},\lambda_1) = \rho D(\mathbf{x},\lambda_2)$ for some *known* positive constant $\rho$, while $\frac{\sigma}{\sqrt{D}}(\mathbf{x},\lambda_1) \neq \frac{\sigma}{\sqrt{D}}(\mathbf{x},\lambda_2)$ for all $\mathbf{x} \in X$.

This assumption essentially requires that the dependence of the diffusion and absorption coefficients is different for at least two wavelengths. Otherwise, we would simply be able to eliminate the spectral dependence from equation (1). We will see later on that this assumption is satisfied by most coefficient models employed by researchers in the community. We also need some assumptions on the regularity and boundary values of the coefficients. We assume, denoting by $\mathcal{C}^p(X)$ the space of $p$-times differentiable functions in $X$, that

(A2) the function $0 < D(\cdot,\lambda) \in \mathcal{C}^2(\bar{X})$, and its boundary value $D_{|\partial X}$ is *known*. The functions $0 < \sigma(\cdot,\lambda), 0 < \Gamma(\cdot,\lambda) \in \mathcal{C}^1(\bar{X})$.

We now present the main uniqueness result on reconstructions with multi-spectral data.

**Theorem 2.1.** *Let* $(D,\sigma,\Gamma)$ *and* $(\tilde{D},\tilde{\sigma},\tilde{\Gamma})$ *be two sets of coefficients given in (3), with* $\gamma(\lambda)$ *known, satisfying assumptions* (A1) *and* (A2). *Then there exists an open set of illuminations* $\big(g_1(\mathbf{x},\lambda),\ g_2(\mathbf{x},\lambda)\big)$ *such that the equality of the data*

$$\{H_1(\mathbf{x},\lambda),\ H_2(\mathbf{x},\lambda)\} = \{\tilde{H}_1(\mathbf{x},\lambda),\ \tilde{H}_2(\mathbf{x},\lambda)\}$$

*in* $X \times \Lambda$ *implies that*

$$\{D(\mathbf{x},\lambda),\ \sigma(\mathbf{x},\lambda),\ \Gamma(\mathbf{x})\} = \{\tilde{D}(\mathbf{x},\lambda),\ \tilde{\sigma}(\mathbf{x},\lambda),\ \tilde{\Gamma}(\mathbf{x})\}$$

*in* $X \times \Lambda$ *provided that the values of the diffusion coefficient agree on the boundary:* $D_{|\partial X} = \tilde{D}_{|\partial X}$ *for all* $\lambda \in \Lambda$.

**Proof.** With the regularity assumptions on the diffusion coefficient, we can recast equation (1), using the Liouville transform $v = \sqrt{D}u$, as

$$\begin{aligned} &\Delta v(\mathbf{x},\lambda) + q(\mathbf{x},\lambda)v(\mathbf{x},\lambda) = 0, && X \times \Lambda \\ &v(\mathbf{x},\lambda) = \tilde{g}(\mathbf{x},\lambda) := \sqrt{D}(\mathbf{x},\lambda)g(\mathbf{x},\lambda), && \partial X \times \Lambda, \end{aligned} \tag{4}$$

with the interior data $H(\mathbf{x},\lambda) = v(\mathbf{x},\lambda)/\chi(\mathbf{x},\lambda)$, where $\chi$ and $q$ are defined respectively as

$$\chi = \frac{\sqrt{D}}{\Gamma\sigma}, \qquad -q = \frac{\Delta\sqrt{D}}{\sqrt{D}} + \frac{\sigma}{D}. \tag{5}$$

Let us denote by $v_1(\mathbf{x},\lambda)$ and $v_2(\mathbf{x},\lambda)$ the solutions of (4) with the illuminations $\tilde{g}_1(\mathbf{x},\lambda)$ and $\tilde{g}_2(\mathbf{x},\lambda)$, respectively. Then it is straightforward to check that [9]

$$\begin{aligned} &-\nabla\cdot v_1^2\nabla\frac{v_2}{v_1} = 0, && X \times \Lambda \\ &v_1^2(\mathbf{x},\lambda) = \tilde{g}_1^2, && \partial X \times \Lambda. \end{aligned} \tag{6}$$

Since $\frac{v_2}{v_1} = \frac{H_2}{H_1}$ is known, this is a transport equation for $v_1^2(\mathbf{x}, \lambda)$ with the vector field $\nabla \frac{H_2}{H_1}$. By the results of [9], there exist the well-chosen illuminations $g_1$ and $g_2$ (and thus $\tilde{g}_1$ and $\tilde{g}_2$) such that the vector field is smooth enough with the positive modulus $|\nabla \frac{H_2}{H_1}| > 0$. This ensures that the transport equation is uniquely solvable for $v_1^2$. Once $v_1^2$ is reconstructed, we can reconstruct $\chi = v_1/H_1$ and then $q = -\Delta v_1/v_1$.

Now let $\lambda_1, \lambda_2 \in \Lambda$ be two wavelengths as in assumption (A1). We first reconstruct the two pairs of functionals $(\chi(\mathbf{x}, \lambda_1),\ q(\mathbf{x}, \lambda_1))$ and $(\chi(\mathbf{x}, \lambda_2),\ q(\mathbf{x}, \lambda_2))$. With the assumption that $D(\mathbf{x}, \lambda_1) = \rho D(\mathbf{x}, \lambda_2)$, we obtain after some algebra using the above equations that

$$\begin{aligned} &\Delta\sqrt{D}(\mathbf{x}, \lambda_1) + Q(\mathbf{x})\sqrt{D}(\mathbf{x}, \lambda_1) = 0, \quad && X \\ &\sqrt{D}(\mathbf{x}, \lambda_1) = \sqrt{D}(\mathbf{x}, \lambda_1)_{|\partial X}, && \partial X, \end{aligned} \tag{7}$$

where the function $Q(\mathbf{x})$ is defined as

$$Q(\mathbf{x}) = \frac{\gamma(\lambda_1)\chi(\mathbf{x}, \lambda_1)q(\mathbf{x}, \lambda_1) - \sqrt{\rho}\gamma(\lambda_2)\chi(\mathbf{x}, \lambda_2)q(\mathbf{x}, \lambda_2)}{\gamma(\lambda_1)\chi(\mathbf{x}, \lambda_1) - \sqrt{\rho}\gamma(\lambda_2)\chi(\mathbf{x}, \lambda_2)}. \tag{8}$$

Using the conditions in assumptions (A1) and (A2), the denominator in $Q$ does not vanish and $Q$ is bounded. The elliptic equation (7) can then be solved uniquely as shown in [9] to reconstruct $\sqrt{D}(\mathbf{x}, \lambda_1)$. We then find

$$\sigma(\mathbf{x}, \lambda_1) = -(Dq)(\mathbf{x}, \lambda_1) - (\sqrt{D}\Delta\sqrt{D})(\mathbf{x}, \lambda_1), \tag{9}$$

$$\Gamma(\mathbf{x}) = \frac{\sqrt{D}(\mathbf{x}, \lambda_1)}{\chi(\mathbf{x}, \lambda_1)\sigma(\mathbf{x}, \lambda_1)}. \tag{10}$$

Once $\Gamma(\mathbf{x})$ is reconstructed, then so is $\Gamma(\mathbf{x}, \lambda) = \Gamma(\mathbf{x})\gamma(\lambda)$. The results in [9, corollary 2.3] then allow us to reconstruct $D(\mathbf{x}, \lambda)$ and $\sigma(\mathbf{x}, \lambda)$ for all $\lambda \in \Lambda$. □

It has been shown in [9] that the reconstruction of $v_1$ (and thus that of $\chi$ and $q$ as well) is Lipschitz stable for each fixed wavelength. Because the solution of (7) is stable with respect to $Q$, we deduce that the reconstruction of the $D(\mathbf{x}, \lambda_1)$ (and thus $\Gamma(\mathbf{x})$) is stable. Precise stability estimates similar to those in [9, theorem 2.4] can be derived.

The coefficient model (3) is quite general and covers many of the models used in the literature. For instance, we may consider the following standard model [13–15, 17, 19, 29, 35, 41, 42, 48, 49, 54, 58, 60]:

$$\begin{aligned} &D(\mathbf{x}, \lambda) = \alpha(\lambda)D(\mathbf{x}), \quad \Gamma(\mathbf{x}, \lambda) = \gamma(\lambda)\Gamma(\mathbf{x}) \\ &\sigma(\mathbf{x}, \lambda) = \sum_{k=1}^{K} \beta_k(\lambda)\sigma_k(\mathbf{x}), \end{aligned} \tag{11}$$

where the functions $\alpha(\lambda)$, $\{\beta_k(\lambda)\}_{k=1}^K$ and $\gamma(\lambda)$ are assumed to be *known*. In other words, all three-coefficient functions can be written as products of functions of different variables. Moreover, the absorption coefficient contains multiple components. This is the parameter model proposed in [17, 19, 29, 35, 42, 49] to reconstruct chromophore/fluorochrome concentrations from optical measurements. The following result regarding model (11) is a natural extension of theorem 2.1.

**Corollary 2.2.** *Let $D(\mathbf{x}, \lambda)$, $\sigma(\mathbf{x}, \lambda)$ and $\Gamma(\mathbf{x}, \lambda)$ be as in (11) and satisfying assumptions* (A1) *and* (A2). *Assume further that there exist $K$ wavelengths such that the matrix $B$ with elements $B_{kj} = \beta_k(\lambda_j)$ $(1 \leqslant k, j \leqslant K)$ is non-singular. Then the coefficients*

$$\{D(\mathbf{x}),\ \{\sigma_k(\mathbf{x})\}_{k=1}^K,\ \Gamma(\mathbf{x})\}$$

*can be uniquely reconstructed from the well-chosen data $(H_1(\mathbf{x}, \lambda), H_2(\mathbf{x}, \lambda))$, $(\mathbf{x}, \lambda) \in X \times \Lambda$.*

**Proof.** Theorem 2.1 allows the unique reconstruction of $D(\mathbf{x})$, $\Gamma(\mathbf{x})$ and $\{\sigma(\mathbf{x}, \lambda_k)\}_{k=1}^K$. Since $B$ is non-singular, we can invert the linear system $\sigma(\mathbf{x}, \lambda_j) = \sum_{k=1}^K \beta_k(\lambda_j)\sigma_k(\mathbf{x})$, $j = 1, \ldots, K$, to recover $\{\sigma_k(\mathbf{x})\}_{k=1}^K$. □

## 3. Reconstruction methods

We now present two numerical reconstruction methods for the multi-spectral qPAT problem.

### *3.1. The vector field method*

The first method is based on the constructive uniqueness proof in the previous section. The proof provides an explicit procedure to reconstruct the unknown coefficients. The main step is to solve the transport equation (6) for $v_1^2$. Let us denote by $\{\lambda_j\}_{j=1}^K$ the wavelengths at which data are measured. For a general pair of coefficients of the form (3) that satisfy assumptions (A1) and (A2), the algorithm proceeds as follows.

*The vector field algorithm*

Step 1. Solve the transport equation (6) for $v_1(\mathbf{x}, \lambda_1)$ and $v_1(\mathbf{x}, \lambda_2)$.
Step 2. Construct $\big(\chi(\mathbf{x}, \lambda_1), q(\mathbf{x}, \lambda_1)\big)$ and $\big(\chi(\mathbf{x}, \lambda_2), q(\mathbf{x}, \lambda_2)\big)$ as

$$\chi(\mathbf{x}, \lambda_j) = \frac{v_1(\mathbf{x}, \lambda_j)}{H_1(\mathbf{x}, \lambda_j)}, \quad q(\mathbf{x}, \lambda_j) = -\frac{\Delta\mathcal{K}(v_1)(\mathbf{x}, \lambda_j)}{v_1(\mathbf{x}, \lambda_j)}, \quad j = 1, 2. \tag{12}$$

Step 3. Construct $Q(\mathbf{x})$ as defined in (8) and solve the elliptic equation (7) for $\sqrt{D(\mathbf{x}, \lambda_1)}$.
Step 4. Recover $\sigma(\mathbf{x}, \lambda_1)$ and $\Gamma(\mathbf{x})$ from formulas (9) and (10).
Step 5. Recover $\big(D(\mathbf{x}, \lambda_2), \sigma(\mathbf{x}, \lambda_2)\big)$ from $\big(\chi(\mathbf{x}, \lambda_2), q(\mathbf{x}, \lambda_2)\big)$.
Step 6. Solve for $\big(D(\mathbf{x}, \lambda_j), \sigma(\mathbf{x}, \lambda_j)\big)$ by repeating the following steps for $3 \leqslant j \leqslant K$.

Step 6(a). Solve the transport equation (6) for $v_1(\mathbf{x}, \lambda_j)$.
Step 6(b). Solve the following elliptic equation for $1/u_1(\mathbf{x}, \lambda_j)$:

$$\nabla \cdot v_1^2 \nabla \frac{1}{u_1} + \frac{H(\mathbf{x}, \lambda_j)}{\gamma(\lambda_j)\Gamma(\mathbf{x})} = 0, \quad \text{in } X, \qquad \frac{1}{u_1} = \frac{1}{g_1(\mathbf{x}, \lambda_j)}, \quad \text{on } \partial X. \tag{13}$$

Step 6(c). Reconstruct $\sigma(\mathbf{x}, \lambda_j) = \frac{H_1(\mathbf{x}, \lambda_j)}{u_1(\mathbf{x}, \lambda_j)}$ and $D(\mathbf{x}, \lambda_j) = \frac{v_1^2(\mathbf{x}, \lambda_j)}{u_1^2(\mathbf{x}, \lambda_j)}$.

Step 6 is the main algorithm that we used in [9] for solving the mono-spectral qPAT problem for the case when $\Gamma(\mathbf{x})$ is known. Equation (13) is obtained by rewriting the diffusion equation (1) for $u_1$ using the fact that $Du_1^2 = v_1^2$. As long as $g_1 \geqslant c_0 > 0$ everywhere on the boundary, this elliptic problem is well-posed for $1/u_1$. For more details on the vector field method in the mono-spectral case, including the discussion on dealing with noisy data, we refer to [9].

The same algorithm can be used when the simplified coefficient model (11) is considered. In that case, step 6(b) is not needed anymore. This is because once $D(\mathbf{x})$ and $\Gamma(\mathbf{x})$ in (11) are reconstructed, $\sigma(\mathbf{x}, \lambda_j)$ $(1 \leqslant j \leqslant K)$ can be reconstructed from the solution $\chi(\mathbf{x}, \lambda_j)$ to the transport equation.

The uniqueness results we presented hold only for coefficients that are regular enough, satisfying the regularity assumptions in (A2). So is this vector field algorithm that we just described. In practice, we do not know *a priori* whether or not the coefficients to be reconstructed satisfy this assumption. We thus have to make sure that $v = \sqrt{D}u$ is smooth enough so that we can take the second-order derivatives without problem. That is the reason we

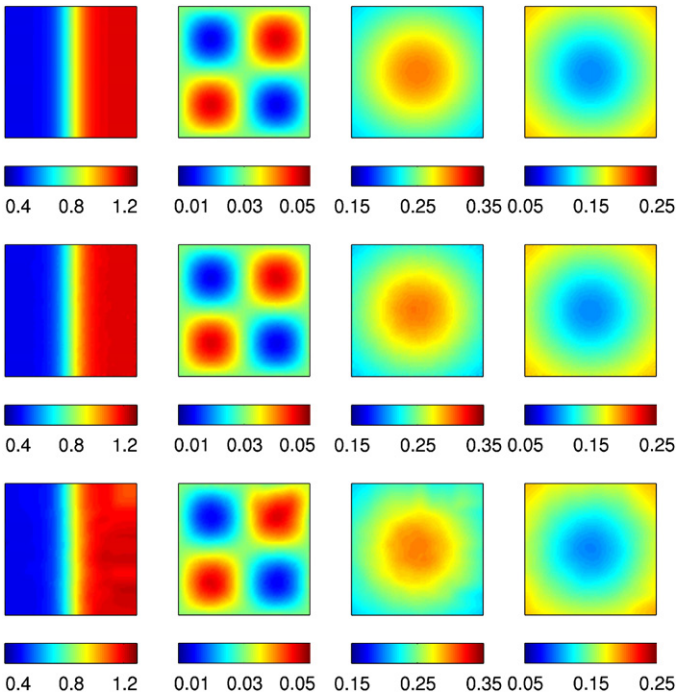


**Figure 1.** The reconstructions of the coefficients ($\Gamma(\mathbf{x})$, $D(\mathbf{x})$, $\sigma_1(\mathbf{x})$, $\sigma_2(\mathbf{x})$). From top to bottom: true coefficients, reconstructions with clean data and reconstructions with data containing 5% random noise.

added a smoothing process to $v$ in step 2 of the algorithm. The kernel $k(\mathbf{x})$ of the convolution operator $\mathcal{K}(v)(\mathbf{x}, \lambda) = \int_X k(\mathbf{x} - \mathbf{y})v(\mathbf{y}, \lambda)\, d\mathbf{y}$ is a smooth function. Here we take $k(\mathbf{x})$ to be a Gaussian whose variance is used to control the strength of the smoothing. The strength of the smoothing is determined by looking at the image of $\Delta\mathcal{K}(v)$. The smoothing, however, does not cause many problems for the solution of the next elliptic problem as we know that the solution of the elliptic problem is stable with respect to changes in $Q$.

### *3.2. The nonlinear least-squares method*

The second approach to solve numerically the inverse problem is to reformulate the reconstruction problem as a data-driven minimization problem. More precisely, we look for the coefficients in the form of (3) that minimize the following mismatch functional:

$$\Phi(D, \sigma, \Gamma) = \frac{1}{2}\sum_{i=1}^{N}\int_X\int_\Lambda \left(H_i(\mathbf{x}, \lambda) - H_i^*(\mathbf{x}, \lambda)\right)^2 d\mathbf{x}\, d\lambda, \tag{14}$$

where $N \geqslant 2$ is the number of different spatial source patterns used for a fixed wavelength. In the theoretical results we presented in section 2, $N = 2$. The data predicted by the model are denoted as $H_i(\mathbf{x}, \lambda) = \Gamma(\mathbf{x}, \lambda)\sigma(\mathbf{x}, \lambda)u_i(\mathbf{x}, \lambda)$, with $u_i(\mathbf{x}, \lambda)$ being the solution of the diffusion equation (1) with the $i$th source pattern $g_i(\mathbf{x}, \lambda)$. The real interior data, that is, the data constructed from acoustic measurement, are denoted by $H_i^*(\mathbf{x}, \lambda)$.

We solve the minimization problem by a quasi-Newton method with the BFGS updating rule on the Hessian operator [12, 30, 38, 44]. This method requires the Fréchet derivatives of

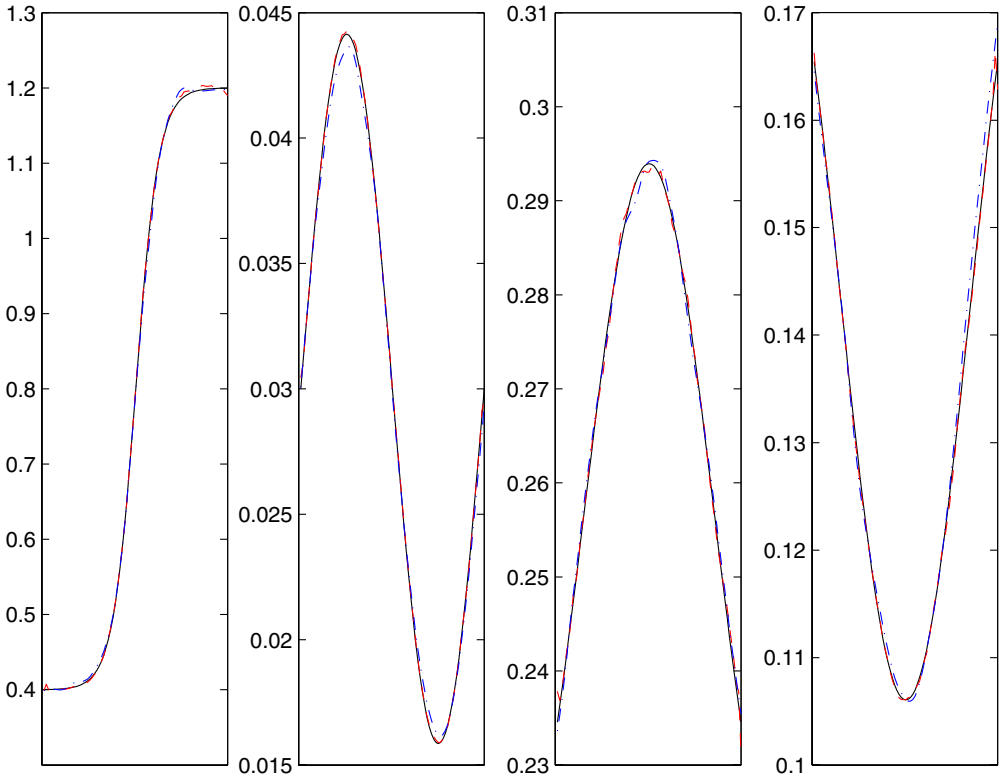


**Figure 2.** Cross-sections of plots in figure 1 along the axis $y = 0.75$. Shown are true coefficients (solid line), reconstruction with noise-free data (red dashed) and reconstructions with noisy data (blue dashed).

the functional $\Phi$ with respect to the unknowns $D, \sigma$ and $\Gamma$. These derivatives can be computed in the following way. Let us denote by $w_i(\mathbf{x}, \lambda)$ the solution of the adjoint problem

$$\begin{aligned} &-\nabla \cdot D(\mathbf{x}, \lambda)\nabla w_i(\mathbf{x}, \lambda) + \sigma(\mathbf{x}, \lambda) w_i = \Gamma \sigma Z_i, \quad X \times \Lambda \\ &w_i(\mathbf{x}, \lambda) = 0, \quad \partial X \times \Lambda, \end{aligned} \tag{15}$$

with $Z_i \equiv H_i(\mathbf{x}, \lambda) - H_i^*(\mathbf{x}, \lambda)$. Then it is standard to show that

**Theorem 3.1.** *The nonlinear least-squares functional $\Phi : [L^2(X \times \Lambda)]^3 \mapsto \mathbb{R}$ is Fréchet differentiable with respect to $D$, $\sigma$ and $\Gamma$. The Fréchet derivatives are given respectively by*

$$\left\langle \frac{\partial \Phi}{\partial D}, \hat{D} \right\rangle = \sum_{i=1}^{N} \langle \nabla u_i \cdot \nabla w_i, \hat{D} \rangle_{L^2(X\times\Lambda)}, \tag{16}$$

$$\left\langle \frac{\partial \Phi}{\partial \Gamma}, \hat{\Gamma} \right\rangle = \sum_{i=1}^{N} \langle Z_i \sigma u_i, \hat{\Gamma} \rangle_{L^2(X\times\Lambda)}, \tag{17}$$

$$\left\langle \frac{\partial \Phi}{\partial \sigma}, \hat{\sigma} \right\rangle = \sum_{i=1}^{N} \langle \Gamma Z_i u_i - w_i u_i, \hat{\sigma} \rangle_{L^2(X\times\Lambda),} \tag{18}$$

*where $\langle \cdot \rangle_{L^2(X\times\Lambda)}$ denotes the usual inner product in $L^2(X \times \Lambda)$.*

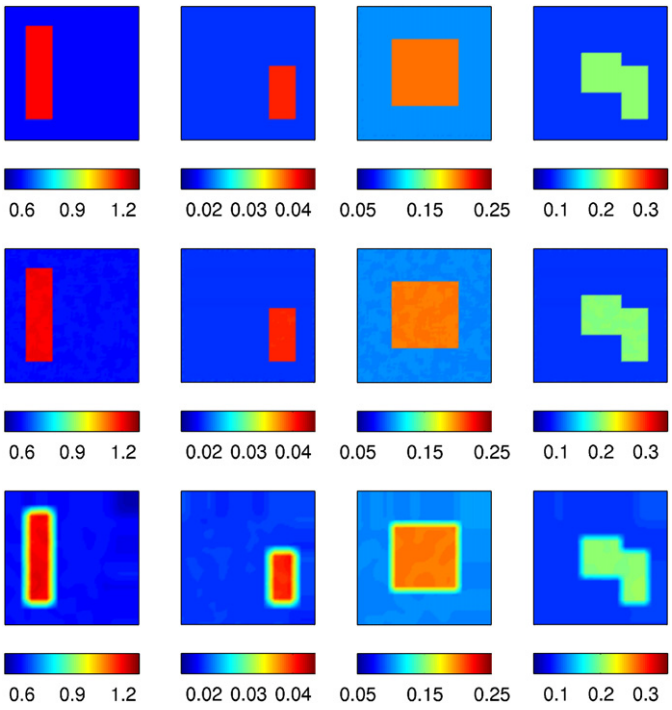


**Figure 3.** The reconstructions of piecewise constant coefficients ($\Gamma(\mathbf{x})$, $D(\mathbf{x})$, $\sigma_1(\mathbf{x})$, $\sigma_2(\mathbf{x})$). From top to bottom: true coefficients, reconstructions with clean data and reconstructions with data containing 5% random noise.

When model (11) is employed, the derivatives with respect to $\sigma$ have to be replaced by the derivatives with respect to each $\sigma_k$ ($1 \leqslant k \leqslant K$). These derivatives can be simply computed by using (18) and the chain rule. More precisely,

$$\left\langle \frac{\partial \Phi}{\partial \sigma_k}, \hat{\sigma}_k \right\rangle = \sum_{i=1}^{N} \langle \Gamma Z_i u_i - w_i u_i, \beta_k(\lambda)\hat{\sigma}_k \rangle_{L^2(X\times\Lambda)}, \quad 1 \leqslant k \leqslant K. \tag{19}$$

Compared with the vector field method in the previous section, the nonlinear least-squares method is a very general method. However, it is computationally more expensive. In each quasi-Newton iteration, we need to solve several forward and adjoint problems to evaluate the value of the objective function and the Fréchet derivatives. The method is thus slow. However, since the diffusion equation (1) and its adjoint (15) are elliptic problems that can be solved efficiently with finite-element methods, the overall reconstruction cost is reasonably low.

## 4. Numerical simulations

We now present some numerical simulations using synthetic data to support the theory that is developed in the previous section. To simplify the presentation, we consider only two-dimensional problems, even though the uniqueness results and the reconstruction methods hold in three-dimensional domains as well. The domain we consider is the square: $X = (0,\ 2\ \text{cm}) \times (0,\ 2\ \text{cm})$. Material properties of the medium will be provided in specific cases.

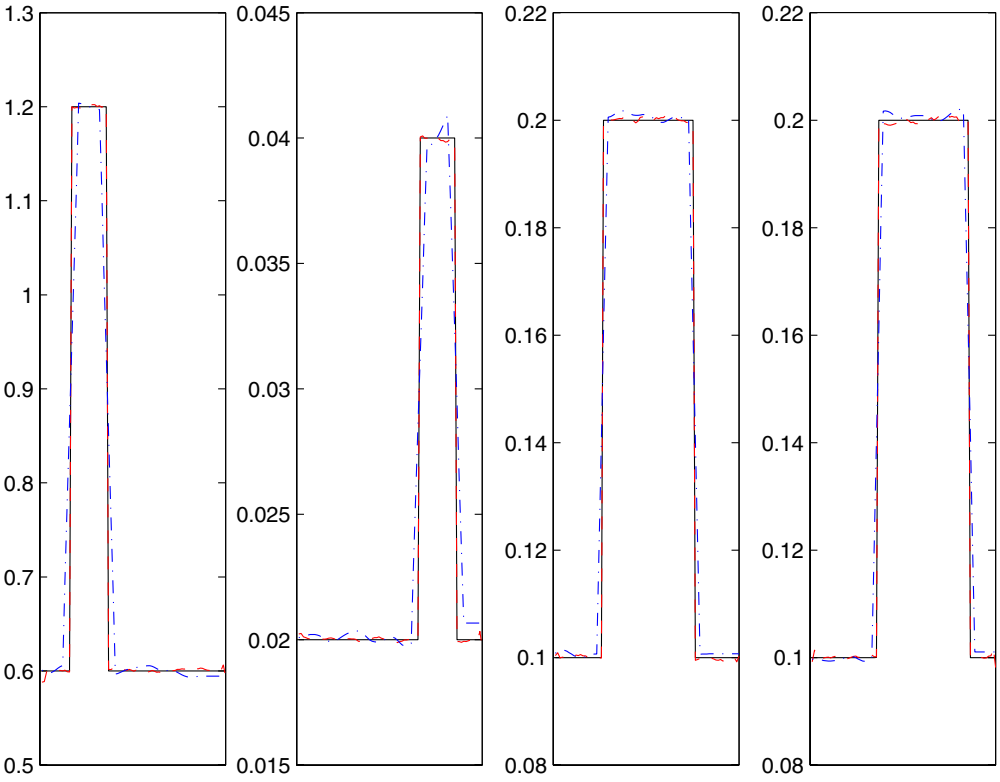


**Figure 4.** Cross-sections of true coefficients (solid line) and the reconstructed coefficients with noise-free data (red dashed) and a typical realization of noisy data (blue dashed) in figure 3 along the axis $y = 1.0$.

In the first set of numerical experiments, we show reconstruction results for smooth coefficients. The coefficients take the forms given in (11) with two components in the absorption coefficient, i.e. $K = 2$. The spectral components of the coefficients are given as follows:

$$\alpha(\lambda) = \left(\frac{\lambda}{\lambda_0}\right)^{3/2}, \quad \gamma(\lambda) = 1, \quad \beta_1(\lambda) = \frac{\lambda}{\lambda_0}, \quad \beta_2(\lambda) = \frac{\lambda_0}{\lambda}, \tag{20}$$

where the normalization wavelength $\lambda_0$ is included to control the amplitude of coefficients. These weight functions are by no means what they should exactly be in practical applications. However, the specific forms do not have impacts on the results of the reconstruction. The spatial components of the coefficients are given as

$$\begin{aligned} &\Gamma(\mathbf{x}) = 0.8 + 0.4\tanh(4x - 4), && D(\mathbf{x}) = 0.03 + 0.02\sin(\pi x)\sin(\pi y) \\ &\sigma_1(\mathbf{x}) = 0.2 + 0.1\mathrm{e}^{-(x-1)^2-(y-1)^2}, && \sigma_2(\mathbf{x}) = 0.2 - 0.1\mathrm{e}^{-(x-1)^2-(y-1)^2}. \end{aligned} \tag{21}$$

Four illuminations are used, two at each wavelength. The reconstruction results with clean data, i.e. synthetic data without being polluted by additional random noise, are shown in the second row of figure 1. Note that the data used in this case indeed contain noise that comes from the discretization of the continuous PDE model, which is very small since we used a very fine discretization. The reconstructions are almost perfect, with overall quality very similar to those presented in mono-spectral data [9], as can be seen from the plots and the cross-sections (red dashed) in figure 2. The third row of figure 1 presents one typical

realization of reconstruction results with data containing 5% extra additive random noise. The cross-sections of the reconstruction along the line $y = 1$ are shown in figure 2 (blue dashed). The results are still very accurate, with overall quality comparable to those results obtained in [9].

In the second set of numerical experiments, we show reconstruction results for piecewise constant coefficients with the numerical minimization algorithm that we introduced in the previous section. The true coefficients are shown in the first row of figure 3. We again use four illuminations of two different wavelengths. The reconstructions with clean and noisy data are presented on the second and third rows of figure 3, respectively. In the case of noisy data, we regularized the nonlinear least-squares problem with the Tikhonov regularization term $\frac{\rho}{2}(\|\nabla D\|^2_{L^2} + \|\nabla\sigma\|^2_{L^2} + \|\nabla\Gamma\|^2_{L^2})$. The strength $\rho$ of the regularization is taken after a few tests with different values. The effect of the regularization is mainly to smooth out the additive noise in the data. It also smooths out part of the jumps across the interfaces of coefficient discontinuities, as can be seen from the plots in the third row of figure 3. To better visualize the quality of the reconstructions, we again plot the cross-sections of the reconstructed coefficients in figure 4. We observe that discontinuous coefficients can be reconstructed as accurately as smooth coefficients, even though the discontinuity is smeared out in the former case.

## 5. Concluding remarks

We presented in this paper some theoretical results for quantitative photoacoustic tomography with multi-spectral interior data to reconstruct the Grüneisen, absorption and diffusion coefficients simultaneously. We showed the uniqueness of the solution to the inverse problem under minor assumptions on the form of the coefficients. One specific case of practical importance is that, if the dependence of the coefficient on the spatial variable and on the wavelength variable can be separated, the spatial components of all three coefficients can be reconstructed with spectral data uniquely and stably.

We presented a vector field-based algorithm and a general nonlinear least-squares-based method for the numerical reconstruction of smooth and rough coefficients. We showed by numerical simulations that the reconstructions are very accurate for both types of coefficients, assuming that the interior data $H$ constructed from measured acoustic data are accurate enough. The reconstructions are stable with Lipschitz type stability estimates that are identical to those in [9].

The uniqueness results that we obtained in this paper depend on the illuminations that are selected. In other words, uniqueness only holds when appropriate illuminations are used. Fortunately, the characterization of these 'well-selected' illuminations is identical to that presented in [9]. In fact, as pointed out in [9], many illumination pairs that we have used work, in the sense that they generate the data $H_1$ and $H_2$ such that the condition $|\nabla\frac{H_2}{H_1}| > 0$ holds, and thus the transport equation (6) is uniquely and stably solvable.

The results of this paper and [9] are all based on diffusion theory for light propagation in tissues. It is well known that the phase-space radiative transport model [5, 6, 43] is a more accurate light propagation model for this application. Uniqueness and stability results for the transport model have been developed in [8] in the situation where measurements from all possible illuminations are available. Numerical simulations have also been reported [20]. It would be interesting to extend the study in [8] to include an unknown variable Grüneisen coefficient.

## Acknowledgments

We would like to thank Professor Simon Arridge (University College London) for useful discussion on the simplified coefficient model (11) in optical and photoacoustic tomography. KR was supported in part by NSF grant DMS-0914825. GB was supported in part by NSF grants DMS-0554097 and DMS-0804696.

## References

[1] Agranovsky M, Kuchment P and Kunyansky L 2009 On reconstruction formulas and algorithms for the TAT and PAT tomography *Photoacoustic Imaging and Spectroscopy* ed L V Wang (Boca Raton, FL: CRC Press) pp 89–101
[2] Ammari H 2008 *An Introduction to Mathematics of Emerging Biomedical Imaging* (Berlin: Springer)
[3] Ammari H, Bossy E, Jugnon V and Kang H 2010 Mathematical modelling in photo-acoustic imaging of small absorbers *SIAM Rev.* **52** 677–95
[4] Ammari H, Bossy E, Jugnon V and Kang H 2011 Quantitative photo-acoustic imaging of small absorbers *SIAM J. Appl. Math.* **71** 676–93
[5] Arridge S R 1999 Optical tomography in medical imaging *Inverse Problems* **15** R41–93
[6] Bal G 2009 Inverse transport theory and applications *Inverse Problems* **25** 053001
[7] Bal G 2010 Hybrid inverse problems and internal information *Inside Out: Inverse Problems and Applications* (*Mathematical Sciences Research Institute Publications*) ed G Uhlmann (Cambridge: Cambridge University Press)
[8] Bal G, Jollivet A and Jugnon V 2010 Inverse transport theory of photoacoustics *Inverse Problems* **26** 025011
[9] Bal G and Ren K 2011 Multi-source quantitative PAT in diffusive regime *Inverse Problems* **27** 075003
[10] Bal G and Uhlmann G 2010 Inverse diffusion theory of photoacoustics *Inverse Problems* **26** 085010
[11] Banerjee B, Bagchi S, Vasu R M and Roy D 2008 Quatitative photoacoustic tomography from boundary pressure measurements: noniterative recovery of optical absorption coefficient from the reconstructed absorbed energy map *J. Opt. Soc. Am.* A **25** 2347–56
[12] Byrd R H, Lu P, Nocedal J and Zhu C 1995 A limited memory algorithm for bound constrained optimization *SIAM J. Sci. Comput.* **16** 1190–208
[13] Chaudhari A J, Darvas F, Bading J R, Moats R A, Conti P S, Smith D J, Cherry S R and Leahy R M 2005 Hyperspectral and multispectral bioluminescence optical tomography for small animal imaging *Phys. Med. Biol.* **50** 5421–41
[14] Cong A X and Wang G 2006 Multispectral bioluminescence tomography: methodology and simulation *Int. J. Biomed. Imag.* **2006** 57614
[15] Correia T, Gibson A and Hebden J 2010 Identification of the optimal wavelengths for optical topography: a photon measurement density function analysis *J. Biomed. Opt.* **15** 056002
[16] Cox B T, Arridge S R and Beard P C 2007 Photoacoustic tomography with a limited-aperture planar sensor and a reverberant cavity *Inverse Problems* **23** S95–112
[17] Cox B T, Arridge S R and Beard P C 2009 Estimating chromophore distributions from multiwavelength photoacoustic images *J. Opt. Soc. Am.* A **26** 443–55
[18] Cox B T, Arridge S R, Köstli K P and Beard P C 2006 Two-dimensional quantitative photoacoustic image reconstruction of absorption distributions in scattering media by use of a simple iterative method *Appl. Opt.* **45** 1866–75
[19] Cox B T, Laufer J G and Beard P C 2009 The challenges for quantitative photoacoustic imaging *Proc. SPIE* **7177** 717713
[20] Cox B T, Tarvainen T and Arridge S R 2011 Multiple illumination quantitative photoacoustic tomography using transport and diffusion models *Tomography and Inverse Transport Theory* (*Contemporary Mathematics* vol 559) ed G Bal, D Finch, P Kuchment, J Schotland, P Stefanov and G Uhlmann (Providence, RI: American Mathematical Society) pp 1–12
[21] Finch D, Haltmeier M and Rakesh 2007 Inversion of spherical means and the wave equation in even dimensions *SIAM J. Appl. Math.* **68** 392–412
[22] Finch D and Rakesh 2007 The spherical mean operator with centers on a sphere *Inverse Problems* **35** S37–50
[23] Gao H, Osher S and Zhao H 2012 Quantitative photoacoustic tomography *Mathematical Modeling in Biomedical Imaging: II. Optical, Ultrasound and Opto-Acoustic Tomographies* (*Lecture Notes in Mathematics*) ed H Ammari (Berlin: Springer)

[24] Gao H, Zhao H and Osher S 2010 Bregman methods in quantitative photoacoustic tomography *CAM Report* 10-42 UCLA
[25] Haltmeier M, Scherzer O, Burgholzer P and Paltauf G 2004 Thermoacoustic computed tomography with large planer receivers *Inverse Problems* **20** 1663–73
[26] Haltmeier M, Schuster T and Scherzer O 2005 Filtered backprojection for thermoacoustic computed tomography in spherical geometry *Math. Methods Appl. Sci.* **28** 1919–37
[27] Hristova Y 2009 Time reversal in thermoacoustic tomography—an error estimate *Inverse Problems* **25** 055008
[28] Hristova Y, Kuchment P and Nguyen L 2008 Reconstruction and time reversal in thermoacoustic tomography in acoustically homogeneous and inhomogeneous media *Inverse Problems* **24** 055006
[29] Kim H K, Flexman M, Yamashiro D J, Kandel J J and Hielscher A H 2010 PDE-constrained multispectral imaging of tissue chromophores with the equation of radiative transfer *Biomed. Opt. Express* **1** 812–24
[30] Klose A D and Hielscher A H 2003 Quasi-Newton methods in optical tomographic image reconstruction *Inverse Problems* **19** 387–409
[31] Kuchment P 2012 Mathematics of hybrid imaging: a brief review *The Mathematical Legacy of Leon Ehrenpreis* ed I Sabadini and D Struppa (Berlin: Springer)
[32] Kuchment P and Kunyansky L 2008 Mathematics of thermoacoustic tomography *Eur. J. Appl. Math.* **19** 191–224
[33] Kuchment P and Kunyansky L 2010 Mathematics of thermoacoustic and photoacoustic tomography *Handbook of Mathematical Methods in Imaging* ed O Scherzer (Berlin: Springer) pp 817–66
[34] Kunyansky L A 2007 Explicit inversion formulae for the spherical mean Radon transform *Inverse Problems* **23** 373–83
[35] Laufer J, Cox B T, Zhang E and Beard P 2010 Quantitative determination of chromophore concentrations from 2d photoacoustic images using a nonlinear model-based inversion scheme *Appl. Opt.* **49** 1219–33
[36] Li C and Wang L 2009 Photoacoustic tomography and sensing in biomedicine *Phys. Med. Biol.* **54** R59–97
[37] Nguyen L V 2009 A family of inversion formulas in thermoacoustic tomography *Inverse Probl. Imag.* **3** 649–75
[38] Nocedal J and Wright S J 1999 *Numerical Optimization* (New York: Springer)
[39] Patch S K and Scherzer O 2007 Photo- and thermo- acoustic imaging *Inverse Problems* **23** S1–10
[40] Qian J, Stefanov P, Uhlmann G and Zhao H 2011 An efficient Neumann-series based algorithm for thermoacoustic and photoacoustic tomography with variable sound speed *SIAM J. Imag. Sci.* **4** 850–83
[41] Razansky D, Distel M, Vinegoni C, Ma R, Perrimon N, Köster R W and Ntziachristos V 2009 Multispectral opto-acoustic tomography of deep-seated fluorescent proteins *in vivo* *Nature Photon.* **3** 412–7
[42] Razansky D, Vinegoni C and Ntziachristos V 2007 Multispectral photoacoustic imaging of fluorochromes in small animals *Opt. Lett.* **32** 2891–3
[43] Ren K 2010 Recent developments in numerical techniques for transport-based medical imaging methods *Commun. Comput. Phys.* **8** 1–50
[44] Ren K, Bal G and Hielscher A H 2006 Frequency domain optical tomography based on the equation of radiative transfer *SIAM J. Sci. Comput.* **28** 1463–89
[45] Ren K, Gao H and Zhao H 2012 A hybrid reconstruction method for quantitative photoacoustic imaging submitted
[46] Ripoll J and Ntziachristos V 2005 Quantitative point source photoacoustic inversion formulas for scattering and absorbing media *Phys. Rev.* E **71** 031912
[47] Scherzer O 2010 *Handbook of Mathematical Methods in Imaging* (Berlin: Springer)
[48] Shao P, Cox B T and Zemp R 2011 Estimating optical absorption, scattering, and Grueneisen distributions with multiple-illumination photoacoustic tomography *Appl. Opt.* **50** 3145–54
[49] Srinivasan S, Pogue B W, Jiang S, Dehghani H and Paulsen K D 2005 Spectrally constrained chromophore and scattering near-infrared tomography provides quantitative and robust reconstruction *Appl. Opt.* **44** 1858–69
[50] Stefanov P and Uhlmann G 2009 Thermoacoustic tomography with variable sound speed *Inverse Problems* **25** 075011
[51] Steinhauer D 2009 A reconstruction procedure for thermoacoustic tomography in the case of limited boundary data arXiv:0905.2954
[52] Steinhauer D 2009 A uniqueness theorem for thermoacoustic tomography in the case of limited boundary data arXiv:0902.2838v2
[53] Tittelfitz J 2011 Thermoacoustic tomography in elastic media arXiv:1105.0898v2
[54] Wang J, Davis S C, Srinivasan S, Jiang S, Pogue B W and Paulsen K D 2008 Spectral tomography with diffuse near-infrared light: inclusion of broadband frequency domain spectral data *J. Biomed. Opt.* **13** 041305
[55] Wang L V 2004 Ultrasound-mediated biophotonic imaging: a review of acousto-optical tomography and photo-acoustic tomography *Disease Markers* **19** 123–38
[56] Wang L V 2008 Tutorial on photoacoustic microscopy and computed tomography *IEEE J. Sel. Topics Quantum Electron.* **14** 171–9

[57] Xu M and Wang L V 2006 Photoacoustic imaging in biomedicine *Rev. Sci. Instrum* **77** 041101
[58] Yuan Z and Jiang H 2009 Simultaneous recovery of tissue physiological and acoustic properties and the criteria for wavelength selection in multispectral photoacoustic tomography *Opt. Lett.* **34** 1714–6
[59] Yuan Z, Wang Q and Jiang H 2007 Reconstruction of optical absorption coefficient maps of heterogeneous media by photoacoustic tomography coupled with diffusion equation based regularized Newton method *Opt. Express* **15** 18076–81
[60] Zacharopoulos A D, Svenmarker P, Axelsson J, Schweiger M, Arridge S R and Andersson-Engels S 2009 A matrix-free algorithm for multiple wavelength fluorescence tomography *Opt. Express* **17** 3025–35
[61] Zemp R J 2010 Quantitative photoacoustic tomography with multiple optical sources *Appl. Opt.* **49** 3566–72